Structural Studies of Bulk to Nano-size Niobium Oxides with Correlation to Their Acidity

Hannah T. Kreissl[1], Molly M.J. Li[1], Yung-Kang Peng[1], Keizo Nakagawa[2], Thomas J.N. Hooper[3], John V. Hanna[3], Ashley Shepherd[1], Tai-Sing Wu[4], Yun-Liang Soo[4], S. C. Edman Tsang[1*]

[1]Department of Chemistry, University of Oxford, Oxford, OX1 3QR, United Kingdom
[2]Centre for Membrane and Film Technology, Graduate School of Science, Technology and Innovation, Kobe University, Kobe 657-8501, Japan
[3]Department of Physics, University of Warwick, Coventry, CV4 7AL, United Kingdom
[4] National Synchrotron Radiation Research Center, Hsinchu, Taiwan

ABSTRACT: Hydrated niobium oxides are used as strong solid acids with a wide variety of catalytic applications, yet the correlations between structure and acidity remain unclear. New insights into the structural features giving rise to Lewis and Brønsted acid sites are presently achieved. It appears that Lewis acid sites can arise from lower coordinate NbO_5 and in some cases NbO_4 sites, which are due to the formation of oxygen vacancies in thin and flexible NbO_6 systems. Such structural flexibility of Nb-O systems is particularly pronounced in high surface area nanostructured materials, including few-to monolayer or mesoporous Nb_2O_5*nH_2O synthesized in the presence of stabilizers. Bulk materials on the other hand only possess fewer quantities of acid sites due to lower surface areas and structural rigidity: small numbers of Brønsted acid sites on HNb_3O_8 arise from a protonic structure due to water content, whereas no acid sites are detected for anhydrous crystalline H-Nb_2O_5.

Introduction

Apart from the stoichiometric NbO, NbO_2 and Nb_2O_5 phases niobium oxides also exist in various non-stoichiometric, metastable and mixed phases, making Nb-O systems very complex and difficult to study.[1–3] In terms of structural variety, Nb_2O_5 and its closely related non-stoichiometric structures present the largest group of niobium oxides. Although the Nb/O ratios are very similar, these non-stoichiometric structures differ significantly with respect to their electrical conductivity, refractive index and photoelectric behaviour.[1,4,5] It is well accepted that physicochemical properties of non-stoichiometric structures are highly dependent on their precise structures and thus form the basis for applications of the materials in semiconductor, photovoltaic, solar device and electronic battery industries. Another significant field of use for niobium oxides is photo and acid catalysis. There are a number of nanostructured Nb-O systems claiming further superior performances. [6–10] It is therefore of great interest to obtain information about the relationships between structure and material properties from bulk to nano size.

Due to the Nb oxidation state of +5 where all 4d electrons are shared with the 2p band of oxygen, Nb_2O_5 compounds are generally white powders of low conductivity.[1,4] Further they are structurally based on interconnected NbO_6 octahedra linked by corner- or edge-sharing with different degrees of distortion.[11,12] A great numbers of structures arises from the multiple possibilities of linking the octahedra, as well as from crystallographic shear where mixing of different linkage regions occurs. Another important factor are impurities and oxygen defects leading to deviations from the regular coordination number of six.[1,13–16] The Nb_2O_5 compounds range from crystalline to amorphous, bulk to nano size and anhydrous to hydrated forms. The most common crystalline phases: T-Nb_2O_5, M-Nb_2O_5 and H-Nb_2O_5 phases were named according to the temperatures (low, medium and high, respectively) they are obtained.[5,12] H-Nb_2O_5 is monoclinic and thermodynamically the most stable niobium oxide phase. It consists of layered 3x4 and 3x5 blocks of corner-sharing octahedra with adjacent blocks linked by octahedra edges, and there is one recurring tetrahedral site per unit cell

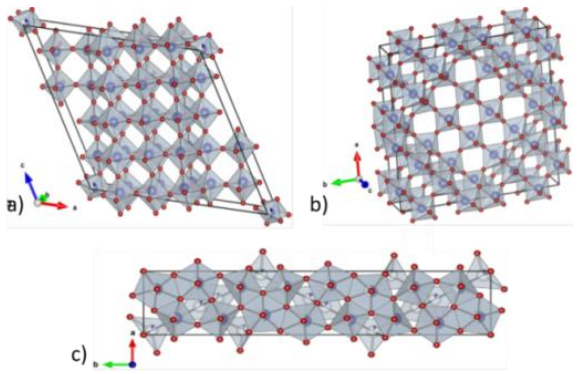

Figure 1. Unit cell structures of common niobium oxides a)H-Nb_2O_5, b)M-Nb_2O_5, c)T-Nb_2O_5 from literature[1]

(Figure 1a).[1,5,17] M-Nb_2O_5 has a tetragonal structure described by 4x4 blocks of corner-sharing octahedra which are linked by edge-sharing octahedra (Figure 1b).[1,5,18] The T-Nb_2O_5 phase is orthorhombic and structurally more complicated, involving six and seven-coordinated Nb atoms which produce distorted octahedra and pentagonal bipyramids, respectively. The polyhedra are linked both by corner- and edge-sharing (Figure 1c).[1,5,19] It is noted that Nb^{5+} is the highest oxidation state for the above Nb-O systems, therefore NbO_6 units as basic structural feature violates Pauling's electrostatic valence rule.[1,20] In addition to the small Nb^{5+} cation size this induces larger structural distortions of the edge- and corner-sharing octahedra in Nb_2O_5 compounds. Crystallographic shear, lattice defects and the introduction of oxygen vacancies are further postulated.[5,13,16] It is however difficult to employ diffraction techniques to confirm the presence of polyhedra and oxygen deficient regions from the structures without their long range order.

Hydrated forms of Nb_2O_5 are also common. The water molecules can be incorporated into the structure by providing O^{2-} as part of the octahedral Nb-O network, while at the same time H^+ acidic sites are formed.[5,21,22] Hydrated niobium oxides have been reported as very strong solid Brønsted acids (BA), containing both terminal and bridging hydroxyls as BA sites. Many of them further contain Lewis acid (LA) sites, which arise from exposure of the Nb centers.[5,9,23,24] Some of these hydrated forms are just denoted as Nb_2O_5*nH_2O, or Nb_2O_5 without reference to the water content, which can sometimes be misleading. For better studied systems information on stoichiometry and structure is available, such as for HNb_3O_8: It has a sheet-like structure consisting of alternating layers of protons and niobates/NbO_6 octahedra connected by edge- and corner-sharing (Figure 2).[8,21,25,26] Due to their strongly acidic character many of these niobium oxides particular in nanometric size can be used as catalysts, for example in esterification, (de)hydration, (de)hydrogenation and redox reactions, etc. They have successfully been applied in the fields of polymer production, photo- and electrochemistry, hydrocarbon conversions and environmental chemistry.[8,10,12,23,24] Unfortunately, the structural details and their relation to acidity remain unclear so far, meaning that targeted synthesis is not yet possible. For a rational design and better catalysts for the different application areas, it is therefore of great interest to study the correlations between structure and acidity in more detail.

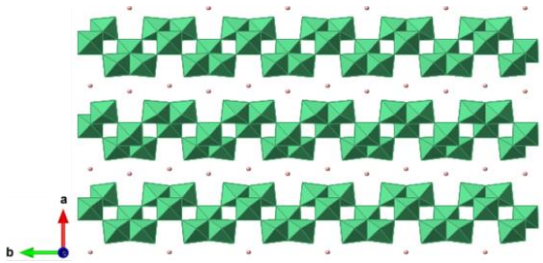

Figure 2. Layered structure of HNb_3O_8 with alternating sheets of interconnected NbO_6 and protons

This paper is focused on the studies of Nb_2O_5 and related hydrated niobium oxides with the help of using various start-of-the-art analytical techniques. Information on structure and morphology is obtained from XRD and TEM, and detailed studies on Nb-O bonding, oxidation states and coordination numbers are performed using Raman spectroscopy, XPS, EXAFS and ^{93}Nb MAS NMR. Combining the results with observations from surface acidity measurements, new insights into structure-acidity correlations are gained. It is found that nanostructured materials of high surface area and structural flexibility, such as few-to monolayer and mesoporous niobium oxides made with the help of stabilizers, possess large amounts of both LA and BA sites. For hydrated bulk materials of low surface area and high crystallinity only BA sites are detected, which are due to the protonic structure formed upon incorporation of water molecules. LA sites on the other hand appear to arise from oxygen vacancies whose formation is based on a significant degree of structural distortion and flexibility.

Experimental

Niobium Oxide Synthesis

A variety of niobium oxides, ranging from bulk to multi- and monolayer structures has been synthesized. The bulk material HNb_3O_8 has been prepared by a conventional solid-state reaction of the precursors K_2CO_3 and Nb_2O_5, followed by proton exchange. Few layer niobium oxide (hy-Nb) and monolayer niobium oxide (hy-Nb-TEOA) have been synthesized hydrothermally from $Nb(OEt)_5$ in ammonia solution, in the case of hy-Nb-TEOA under further addition of triethanolamine (TEOA). Both materials have been acid treated before use, in order to remove the basic surfactant species which block their acid sites. Mesoporous Nb_2O_5*nH_2O (meso Nb_2O_5) has been prepared by hydrolysis and condensation of $Nb(OEt)_5$, followed by soaking in acid solution. Detailed synthetic procedures and references are given in SI. For comparison, commercial bulk Nb_2O_5 (Alfa Aesar) is used.

Characterization

Sample crystallinity was identified by powder XRD using an X' pert Pro (PANalytical) instrument operating in Bragg-Brentano focusing geometry and using Cuka radiation (λ= 1.5418 Å) from a generator operating at 40 kV and 40 mA.

Sample morphology and microstructure were examined by TEM using a JEOL 3000F microscope operated at 300 kV. TEM specimens were prepared by pipetting 5 µl of the sample dispersion in ethanol onto holey carbon-coated copper mesh grids (400 meshes).

Raman spectra were collected on a Perkin Elmer Raman Spectrum 400F using a laser excitation wavelength of 532 nm. 5 scans of exposure time of 10s were taken for each sample. The samples were further dried at 150°C before the measurements.

XPS surface analysis measurements were recorded on a Thermo Scientific K-Alfa XPS instrument equipped with

micro-focused mono-chromated Al X-ray source. The source was operated at 12 keV and a 400 micron spot size was used. The analyzer operated at the energy (CAE) of 200 eV for survey scans and 50 eV for detailed scans. Charge neutralization was applied using a combined low energy/ ion flood source. The data acquisition and analysis were conducted with CasaXPS (Casa software Ltd.). The peak position was referenced to the C1s peak of the carbon tape at 285.00 eV.

Oxidation states and local structures of Nb atoms were probed by X-ray absorption fine structure, XAFS, (beamline BL07A at National Synchrotron Radiation Research Center Taiwan). A Si(111) Double Crystal Monochromator (DCM) was used to scan the photon energy and the energy resolution ($\Delta E/E$) for incident X-ray photons was estimated to be 2×10^{-4}. Transmission mode was adopted for Nb K-edge EXAFS measurements and at least two scan sets were collected and compared for each sample. The data analysis was performed using IFEFFIT with Horae packages (Athena and Artemes). Calibrations and structural refinements were done using Nb metal as a reference. First shell data analyses were performed under the assumption of single scattering with error estimation given by the R-factor.

The ^{93}Nb static NMR measurements were undertaken at 14.1 T using a Bruker Avance II+-600 spectrometer operating at the ^{93}Nb Larmor frequency of 146.66 MHz. All ^{93}Nb NMR data were acquired using a 5 mm static Bruker probe. A $\pi/2$ pulse length was determined on $K[NbCl_6].CH_3CN$ resulting in a selective $\pi/6$ pulse length of 0.5 μs that satisfied the uniform excitation condition for quadrupolar nuclei[27] where $(I+\frac{1}{2})\omega_{rf}t_p \leq \pi/6$. A $(\pi/6)$-τ-$(\pi/6)$ echo sequence was utilised to diminish ringing effects with a τ period of 30 μs and a recycle delay of 0.5 s.[28–30] All ^{93}Nb chemical shifts were referenced to $K[NbCl_6].CH_3CN$ (δ_{iso}=0.0 ppm).

Acid site characterization was conducted using trimethylphospine (TMP) adsorption, followed by ^{31}P MAS NMR (TMP NMR) measurements. The acid type, LA or BA, and acid strength can be differentiated by the ^{31}P chemical shift of TMP due to the variations in interaction strength of the adsorbed TMP molecule with different acid sites. (0 to -6 ppm are typically associated with BA; -20 to -58 ppm with LA; the less negative the shift value, the stronger the acidity). Furthermore, quantitative analysis of the ^{31}P NMR peaks was carried out.[31,32] For a detailed description of the TMP ^{31}P MAS NMR measurements, see SI.

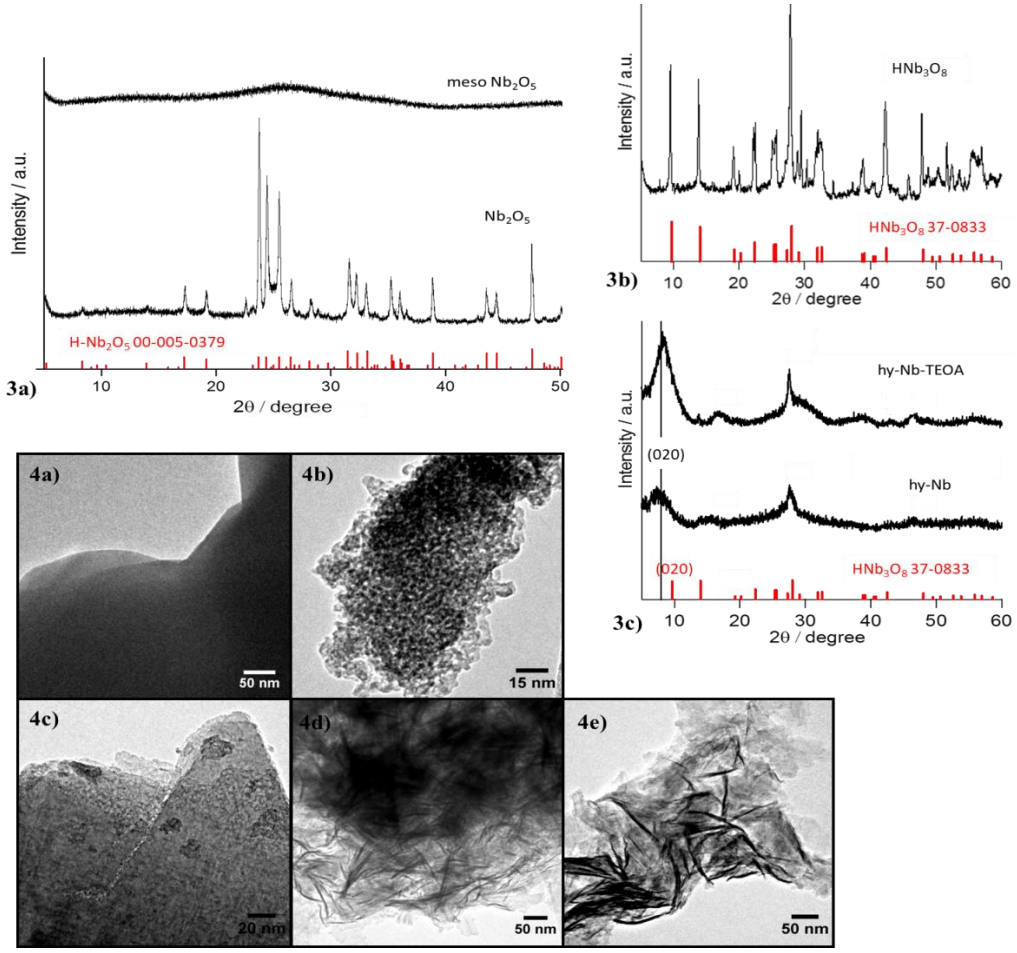

Figure 3. XRD patterns of a) Nb_2O_5 and mesoporous Nb_2O_5*nH_2O, b) HNb_3O_8, c) hy-Nb and hy-Nb-TEOA

Figure 4. TEM images of a) Nb_2O_5, b) mesoporous Nb_2O_5*nH_2O, c) HNb_3O_8, d) hy-Nb, e) hy-Nb-TEOA

Results and Discussion

Comparing the obtained XRD spectra to literature shows that commercial Nb_2O_5 has a crystalline H-Nb_2O_5 structure[1,2] (Figure 3a), the thermodynamically most stable and monoclinic niobium oxide phase which consists primarily of corner- and edge-sharing NbO_6 units. The synthesised HNb_3O_8 also compares well to literature[26,33] (Figure 3b), its crystalline structure is known to consist of alternating layers of protons and niobate sheets made of edge- and corner-sharing NbO_6 units. When it comes to hy-Nb-TEOA and hy-Nb, the XRD spectra are a lot broader, indicating a significant decrease in crystallinity (Figure 3c). The synthesis of these two nano-materials was only recently reported[8] but no structural detail about their Nb-O bonding is yet given. It has however been shown that they consist of many discrete thin layers[8], which is in contrast to bulk Nb_2O_5 and HNb_3O_8, as also seen in the TEM images in Figure 4 (a, c-e). Their layer exfoliation is facilitated by the addition of TEOA or ammonia as stabilizers during hydrothermal synthesis, where the stabilizers might also assist in the reduction of these Nb-O systems. Their XRD spectra suggest that hy-Nb-TEOA and hy-Nb have structural similarities to HNb_3O_8. The peak broadening and shift to lower angles for the (020) diffraction peak, as well as the shift in relative peak intensities can be explained by the increasing interlayer distance and 2D directional orientation when compared to bulk HNb_3O_8 (Figure 3c). Thus, the layer separation results in less rigid and only partially crystalline structures. In the case of mesoporous Nb_2O_5*nH_2O, no structural information can be obtained from the almost flat XRD diffractogram, indicative of its amorphous nature (Figure 3a) although mesoporous structure is shown by TEM and BET/pore analysis (Figure 4b and Figure S1).

From Raman spectroscopy the same trend in sample crystallinity is observed as from XRD: Commercial Nb_2O_5 and bulk HNb_3O_8 give clear peaks indicating higher crystallinity while the broader spectra of hy-Nb and hy-Nb-TEOA indicate lower crystallinity, and finally a very broad spectrum is obtained for the amorphous mesoporous Nb_2O_5*nH_2O (Figure 5). As reported in literature, it is difficult to assign specific Nb-O stretching modes to corresponding frequencies in the Raman spectrum. Especially the frequency ranges between 200 - 400 cm^{-1} and 400 - 760 cm^{-1} do not only correspond to Nb-O stretching modes of long and intermediate bonds but are perturbed by symmetry-related vibrations and coupling between neighbouring entities.[11,20,34,35] The frequency ranges between 760 – 1000 cm^{-1} are better to assign and mostly correspond to the shortest Nb-O bonds in each system. Niobium oxides consisting mainly of corner-shared octahedra tend to have their highest frequency stretching mode in the lower end region of around 800 cm^{-1}.[20,34] This relates to their crystal structure with a lower degree in bond length variation between 1.9 – 2.0 Å and less structural strain. Niobium oxides consisting significantly of edge-shared octahedra, such as H-Nb_2O_5, tend to have their highest frequency stretching mode in the upper

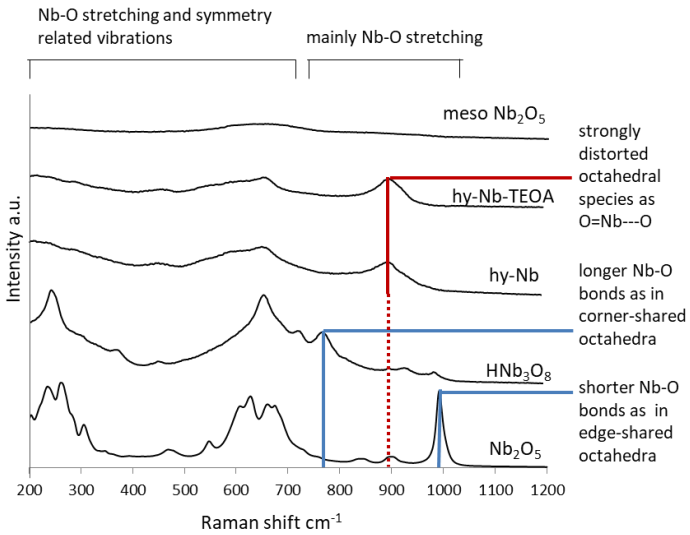

Figure 5. Raman spectra of the different niobium oxides

region of around 1000 cm^{-1}.[20,34,35] This value can be associated with larger bond length variations between 1.73 – 2.26 Å.

By careful examining the Raman spectra of this work (Figure 5), it can be seen that the spectrum of commercial Nb_2O_5 matches well with that of H-Nb_2O_5[11,20,35], thus consistent with the XRD result. A sharp peak is seen at about 1000 cm^{-1}, which arises most likely from the significant amount of edge-sharing NbO_6 with many short Nb-O bonds in a closely packed structure.[11,20] For HNb_3O_8 there is a larger peak at 780 cm^{-1} but only a very small peak at 1000 cm^{-1}, suggesting longer bond lengths and less structural rigidity than for Nb_2O_5. It is known that the crystal structure of HNb_3O_8 consists of considerable amounts of corner- besides edge-sharing octahedra and is further a layered structure with more structural flexibility[8,26,33], which explains the observed longer bond lengths. A significant Raman peak broadening for hy-Nb and hy-Nb-TEOA compared to the crystalline bulk materials HNb_3O_8 and Nb_2O_5 is observed. This is expected from the lower crystallinity and higher structural flexibility of these two materials due to increasing interlayer distances. This supports the previous observations from TEM and XRD. However it is to note that besides a broadening of the typical bond regions an additional large peak is observed around 900 cm^{-1} for both hy-Nb and hy-Nb-TEOA. This peak is not obvious in the spectra of Nb_2O_5 and HNb_3O_8. It implies that there are some structural changes from HNb_3O_8 to hy-Nb and hy-Nb-TEOA. The feature around 900 cm^{-1} is believed to arise from octahedral distortions with species such as O=Nb---O, having a double bond like and a single elongated Nb---O bond as part of the octahedron.[11,20,34] Since the hy-Nb and hy-Nb-TEOA have very high surface areas and structural flexibility due to their layer separations, this octahedral deformation appears to be reasonable. Finally, the Raman spectrum of mesoporous Nb_2O_5*nH_2O is almost flat, with only a very broad peak in the region of 500 – 750 cm^{-1}, were peaks have also

been observed for the other niobium oxides. Unfortunately no further information can be obtained, like-wise to XRD, due to the apparently highly amorphous structure and low symmetry of mesoporous Nb_2O_5*nH_2O.

XPS spectra of the different niobium oxides have been taken as they can give further information about oxidation state and atomic environment. Literature has shown that for niobium compounds the Nb 3d region is generally the most sensitive and characteristic.[36–39] This region always shows peak doublets due to spin-orbit coupling of the Nb 3d orbital, giving rise to a Nb $3d_{5/2}$ and a Nb $3d_{3/2}$ peak with an area ratio of 3:2 and a peak separation of 2.72 eV. The doublet position shifts according to oxidation state, with a higher oxidation state causing a shift towards higher binding energies (BEs).[36,37,40] The BE values representing a sample's Nb 3d region are usually given in form of the Nb $3d_{5/2}$ peak values. Nb_2O_5 with an oxidation state of Nb^{5+} and NbO_2 with an oxidation state of Nb^{4+} have been reported with BE values of about 207.4 eV and 206.2 eV, respectively.[40,41] However, the deviation of BE up to 0.5 eV is not uncommon due to instrumental drift and measurement errors. It is thus more important to compare the measured values relative to each other.

The XPS Nb 3d spectrum of commercial Nb_2O_5 (H-Nb_2O_5) shows a doublet with a binding energy of 207.1 eV, comparing well with the literature values for Nb^{5+} (Figure 6 a.1).[40,41] Since the crystal structure of H-Nb_2O_5 is known to consist of both edge- and corner-sharing octahedra as well as the occasional tetrahedron[1], all of which provide different Nb environments, strictly speaking 3 doublets would be expected: Two large doublets in the Nb^{5+} region and one very small doublet, potentially shifted towards Nb^{4+}. Using an XPS peak fitting program (CasaXPS) it is possible to fit the expected 3 doublets (Figure 6 a.2), however the peak shifts are too small to get mathematical reliable results, the fitting using one doublet is just as good as that of the 3 doublets. This suggests that the corresponding BE's of the three Nb species are too close to separate. The XPS spectrum of HNb_3O_8 shows a similar result to H-Nb_2O_5, giving only one obvious doublet (Figure 6b) despite the fact that two Nb environments are anticipated. As more or less expected from here, the remaining samples of hy-Nb (Figure 6c), hy-Nb-TEOA (Figure 6d) and mesoporous Nb_2O_5*nH_2O (Figure 6e) whose structures remain to be identified, also show only one apparent doublet. It is therefore not possible for XPS to draw conclusions about the number of Nb

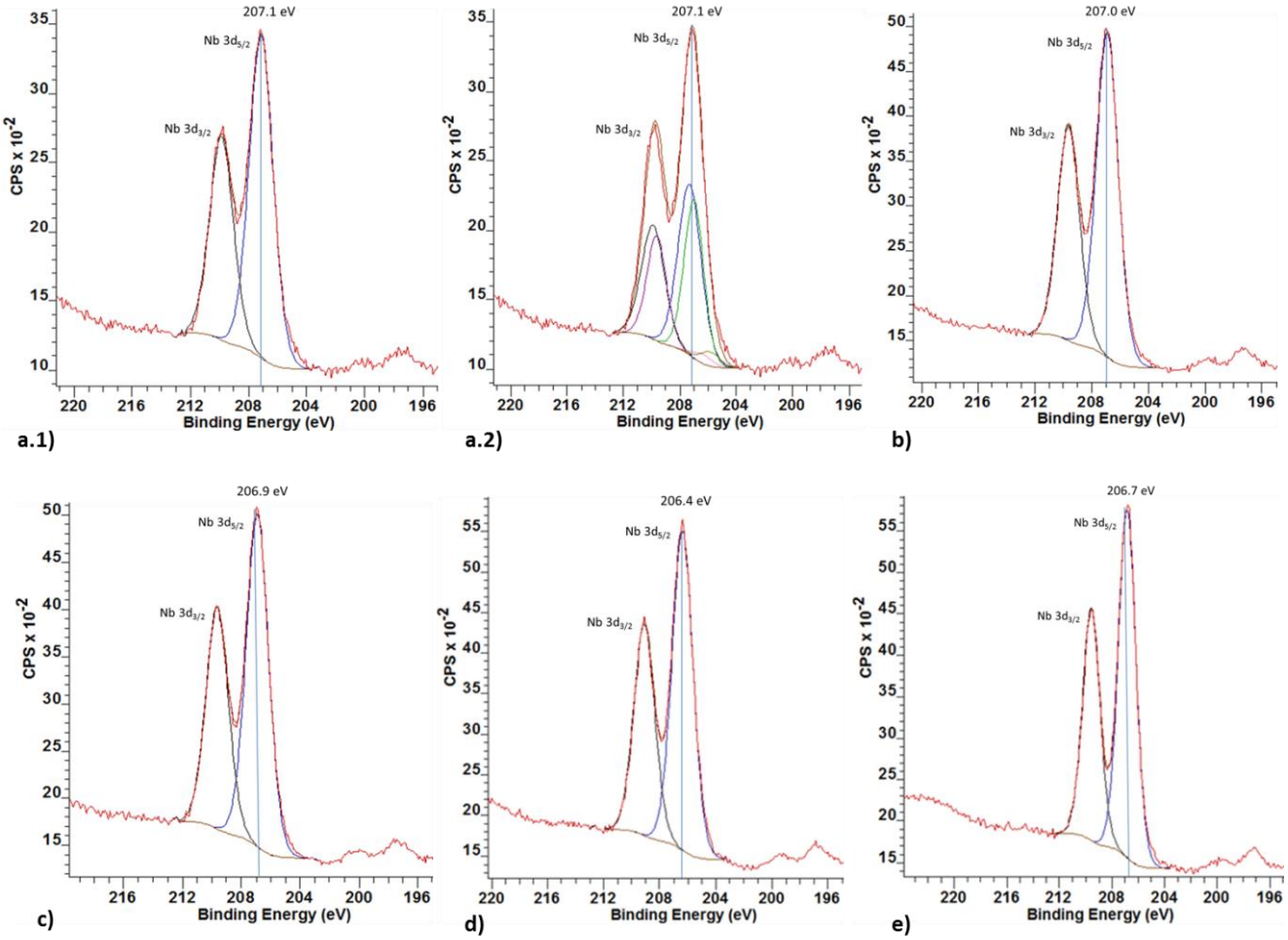

Figure 6. XPS spectra of the different niobium oxides a.1) Nb_2O_5 single doublet fitting, a.2) Nb_2O_5 triple doublet fitting, b) HNb_3O_8, c) hy-Nb, d) hy-Nb-TEOA, e) mesoporous Nb_2O_5*nH_2O

Table 1. Nb 3d peak regions of the niobium oxides

Sample	Nb 3d5/2 peak region (eV)
Nb_2O_5	207.1
HNb_3O_8	207.0
hy-Nb	206.9
hy-Nb-TEOA	206.4
mesoporous Nb_2O_5*nH_2O	206.7

Peak region given as Nb $3d_{5/2}$ peak centre values (common denotation)

environments arising from different extents of octahedral distortion or small coordination changes. However there is one visible difference amongst the niobium oxide samples: the chemical shift of the Nb 3d region (Figure 6 and Table 1). For commercial Nb_2O_5 the Nb 3d5/2 region is centred at 207.1 eV > 207.0 eV for HNb_3O_8 > 206.9 eV for hy-Nb > 206.7 eV for mesoporous Nb_2O_5*nH_2O > 206.4 eV for hy-Nb-TEOA. As seen there is an obvious shift in oxidation state from Nb_2O_5 with mostly Nb^{5+} character to hy-Nb-TEOA with more Nb^{4+} character. A similar shift towards Nb^{4+} has been observed by Xiong et al. who compared their exfoliated/nanosheet-HNb_3O_8 with bulk HNb_3O_8.[26] For the bulk materials Nb_2O_5 and HNb_3O_8 the Nb oxidation state of +5 is expected due to their composition of almost purely edge- and corner-sharing octahedra. Whereas, the few- to monolayered materials hy-Nb and hy-Nb-TEOA having larger structural flexibility and disorder than HNb_3O_8, as previously shown by TEM, XRD and Raman spectroscopy contain a higher contribution of Nb^{4+} (a higher degree of average Nb 3d5/2 peak shift)

It is recalled that Raman spectroscopy suggests the presence of a characteristic distorted O=Nb---O species with one double-bond like and one elongated Nb-O bond. With respect to the apparent XPS BE shift towards Nb^{4+}, this feature in the case of hy-Nb and especially hy-Nb-TEOA might form the structural basis to give rise to oxygen vacancies during synthesis. Some of the distorted and elongated bonds of Nb---O from O=Nb---O can be broken during a reduction process enabled by stabilizers, resulting in an electron-richer five-coordinated Nb^{4+} centre (Scheme 1). It is appreciated that a more pronounced shift towards Nb^{4+} character for hy-Nb-TEOA compared to hy-Nb is due to a higher degree of layer exfoliation by TEOA during the synthesis. This increases its structural flexibility and oxygen vacancy formation. The lower coordination number derived by EXAFS for hy-Nb-TEOA (discussed in the next section) also supports this postulation. Interestingly mesoporous Nb_2O_5*nH_2O with its highly amorphous feature shows a similarly high Nb^{4+} content as hy-Nb and hy-Nb-TEOA.

As a side note, it is interesting to observe the chemical shift towards Nb^{4+} character for hy-Nb-TEOA and mesoporous Nb_2O_5*nH_2O from XPS. The presence of unpaired electrons from Nb^{4+} is expected to give coloured samples, such as in NbO_2 with a blue colour.[1] However, all the niobium oxide samples studied are white in colour, leaving two possible explanations: the amount of Nb^{4+} species could be too small to create a detectible colour. Alternatively, it could be the partial electronic delocalization in the Nb-O networks. Instead of forming individual Nb^{4+} species upon oxygen removal, the electrons might be delocalized amongst the Nb centres in NbO_6 networks. This would also explain why a shift in total oxidation state rather than separate signals from Nb^{5+} and Nb^{4+} are detected in XPS. Such network sharing or building of a superstructure for defects present in large amounts has been suggested for conductive metal oxides in literature.[16,42]

It is noted that we have restrained ourselves from analysing the corresponding O1s spectrum instead of using the Nb 3d to deduce the degree of oxygen vacancies in these materials. It is because the presence of oxygen impurities in carbon tape as the random but significant background gives a non-compensable contribution to the O1s spectrum. This reduces the useful information that can be obtained from O1s analysis.

Scheme 1. Proposed oxygen vacancy formation during synthesis with stabilizers

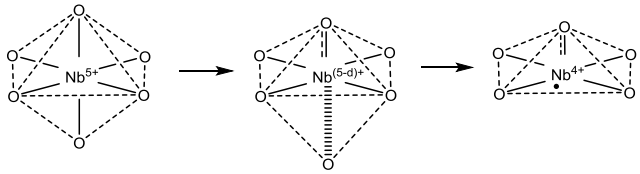

Based on observations from Raman, XPS and EXAFS

For further investigation of the local Nb environment XAFS measurements have been done. The obtained x-ray absorption near edge spectra (XANES) of the Nb K-edge are displayed in Figure 7. Generally, a higher oxidation state causes a shift towards higher absorption energies. But in the case of Nb^{5+} versus Nb^{4+} the energy gap is rather small and may be obscured by the presence of a pre-edge peak and other shape factors.[43,44] It has been reported that Nb^{5+} species as in Nb_2O_5 with a higher oxidation state display a larger pre-edge peak than Nb^{4+} species as in NbO_2.[43,45,46] Although the pre-edge peaks of our measured niobium oxide samples are very close in position, the order of the peak size of Nb_2O_5 > HNb_3O_8 > hy-Nb-TEOA > hy-Nb > mesoporous Nb_2O_5*nH_2O (Figure 7) can be seen. They follow a similar trend as in XPS, however there

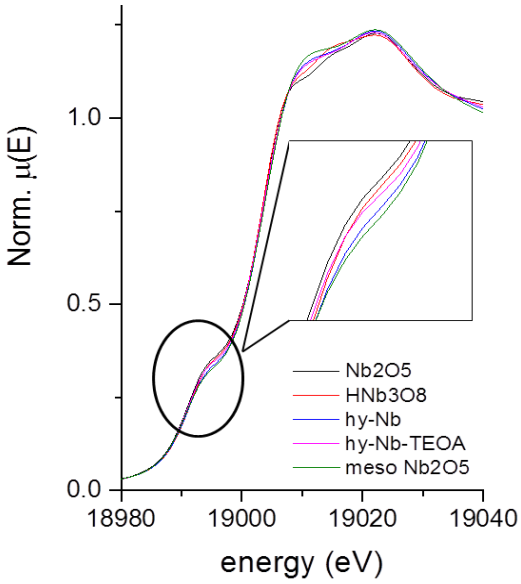

Figure 7. XANES Nb K-edge absorption spectra for the different niobium oxides

are discrepancies in the precise order for the structures of hy-Nb, hy-Nb-TEOA and mesoporous Nb_2O_5*nH_2O. It is to bear in mind that the size of the pre-edge peak is not only dependent on oxidation state but also on the coordination environment.[47,48] In this context it should be mentioned that the average coordination numbers of the few- to monolayer and the porous material are significantly lower than for the bulk materials (Table 2).

Information on bond distances and coordination number can be obtained by analysis of the extended x-ray absorption fine structure (EXAFS).[44–46,49] The fitted k and R ranges for the first neighbours (1st O-shell) of each sample can be found in the Supporting Information, where the R space amplitude relates to the radial distance from Nb at which bonds to neighbouring atoms are present. The calculated Nb-O bond lengths and coordination numbers are displayed in Table 2. For commercial Nb_2O_5 (H-Nb_2O_5) two Nb-O types with bond lengths of 1.76 Å and 1.96 Å are obtained, with respective Nb coordination numbers of 1.4 and 4.3, giving a total of 5.7. The numbers correlate well with the crystal structure of H-Nb_2O_5 that is made mainly of octahedra and very few tetrahedra[1], resulting in an average coordination of just below 6. It has further been reported in literature that corner-sharing octahedra consist of uniform Nb-O bonds of 1.9 – 2.0 Å while the more distorted edge-shared octahedra vary in bond lengths between 1.73 – 2.26 Å.[20,34,44] It appears that the measured Nb-O bonds of 1.76 Å represent the shorter edge-sharing octahedral bonds, while 1.96 Å with a larger average coordination number represents both the longer edge-sharing and the uniform corner-sharing bonds. For HNb_3O_8 two similar Nb-O bond lengths with respective coordination are obtained, plus a third Nb-O bond of

Table 2. Bond distances and coordination numbers for the different niobium oxides

	Scattering path	Bond length in Å	Coordination number	Total Coordination number
Nb_2O_5	Nb-O1	1.76	1.4	5.7
	Nb-O2	1.96	4.3	
HNb_3O_8	Nb-O1	1.77	1.0	6.2
	Nb-O2	2.02	4.1	
	Nb-O3	2.22	1.1	
hy-Nb	Nb-O1	1.88	0.9	5.6
	Nb-O2	2.07	3.8	
	Nb-O3	2.31	0.9	
hy-Nb-TEOA	Nb-O1	1.93	1.1	4.8
	Nb-O2	2.09	3.4	
	Nb-O3	2.29	0.3	
meso Nb_2O_5	Nb-O1	1.91	0.9	4.5
	Nb-O2	2.10	3.6	

Information obtained from EXAFS k and R space transformations with fitting for 1st O-shell

2.22 Å with a coordination of 1.1. The Nb-O bond lengths correlate well with findings on KNb_3O_8, the precursor of HNb_3O_8 from ion exchange, and also with Crystal Maker data of HNb_3O_8, where the larger numbers of given Nb-O bond distances can be grouped to give the bond categories found from EXAFS.[50] The total coordination number is 6.2, correlating well with the layered structure known to consist of NbO_6 sheets with a theoretical coordination of 6. The Nb-O bonds of similar nature to Nb_2O_5 are probably again due to the edge- and corner-sharing octahedra present, while the additional longer bond type likely arises from the layered structure with a gain in flexibility along the z-axis. The overall increase in bond length and structural flexibility for HNb_3O_8 compared to Nb_2O_5 also compares well with the observations from Raman spectroscopy. For hy-Nb the trend in bond lengths and coordination numbers is similar to HNb_3O_8, supporting their structural similarities as shown by XRD. The overall longer Nb-O bonds of hy-Nb are a sign of higher structural flexibility due to layer separation as shown previously. With a total coordination number of below 6 this likely includes the formation of some oxygen vacancies as suggested by XPS. These observations become more apparent for the few- to monolayered hy-Nb-TEOA, with even longer Nb-O bonds and a total coordination number of only 4.8. Interestingly, the percentage of the longest Nb-O bond type (Nb-O3) is largely reduced compared to hy-Nb and HNb_3O_8, suggesting the complete removal of significant amounts of elongated Nb---O bonds. This results in the formation of oxygen vacancies and a greatly distorted structure with reduced average coordination numbers. It goes in line with the XPS observations of an increased Nb^{4+} character for hy-Nb-TEOA (Scheme 1). For mesoporous Nb_2O_5*nH_2O, as for Nb_2O_5, there are only

two types of Nb-O bonds measured with 1.91 Å and 2.10 Å and respective coordination of 0.9 and 3.6. The overall longer bonds compared to Nb_2O_5 suggest a rather loose and flexible packing of structural units, pointing towards corner-sharing NbO_6. With a coordination number of only 4.5, the structure could be a mix of four-, five- and six-coordinated Nb-O units, which would match its amorphous nature (Scheme 2). It is difficult to make a more specific statement on coordination numbers since the calculated numbers present an average and involve fitting limitations.[51]

Scheme 2. Proposed structure of amorphous mesoporous Nb_2O_5*nH_2O

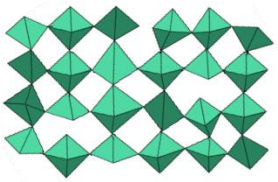

Based on EXAFS and XPS results (protons not shown)

Further comparison can be drawn by observing the ^{93}Nb static broadline NMR data of the niobium oxide samples measured at 14.1 T. The 100% natural abundance, high gyromagnetic ratio and I=9/2 spin number of the ^{93}Nb nucleus are the aspects that are advantageous to these static NMR measurements. However the large convoluted quadrupolar (C_Q) and chemical shift anisotropy (CSA) contributions to these linewidths often lead to a significant broadening of the central transition resonance, even at very high magnetic field strengths. These complex characteristics describing the ^{93}Nb static linewidth often reduce the effectiveness of fast MAS rates when attempting to determine accurate values of the ^{93}Nb NMR parameters.[30,52–54] Octahedrally coordinated NbO_6 environments are normally observed to exhibit δ_{iso} values in the range of ~–900 - –1100 ppm, with quadrupole coupling constants (C_Q) typically ranging from 0-~55 MHz. Four coordinate NbO_4 and five coordinate NbO_5 positions generally possess lower point symmetry and are characterised by more downfield δ_{iso} values in the range of ~–700 - –850 ppm and very large C_Q values of >80 MHz.[30,38,53] The tendency for NbO_4 to assume the reduced Nb^{4+} oxidation state can result in signals which are influenced significantly by paramagnetic broadening and associated paramagnetic shifts.[55]

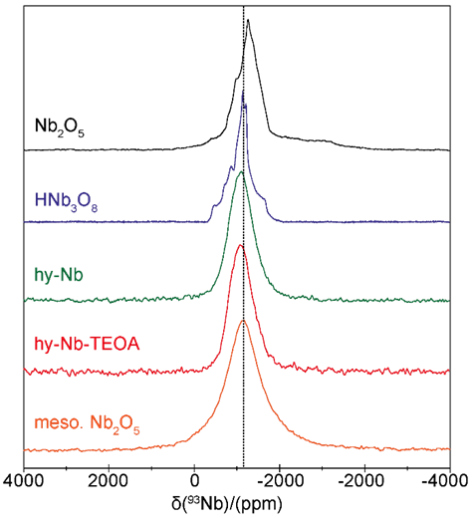

Figure 8. ^{93}Nb static NMR spectra of the different niobium oxides with a dotted line through the centre-of-gravity position (δ_{CG}) of mesoporous Nb_2O_5*nH_2O

The static broadline ^{93}Nb NMR data for the niobium oxide samples is shown in Figure 8. On first inspection it is apparent that Nb_2O_5 exhibits more distinct lineshape features than the remaining samples. The HNb_3O_8 spectrum is consistent with that previously reported, where it has been shown to consist of two quadrupolar/CSA broadened resonances assigned to the two chemically distinct edge-sharing and corner-sharing NbO_6 positions.[38] The Nb_2O_5 lineshape is broader and less well defined than that for its HNb_3O_8 counterpart. This is in agreement with previous studies which have demonstrated that a larger number of non-equivalent Nb sites is a specific feature of Nb_2O_5 phases, and that numerous overlapping NbO_6 subspectra comprise the static ^{93}Nb NMR lineshape.[30] The ^{93}Nb spectra for hy-Nb, hy-Nb-TEOA and mesoporous Nb_2O_5*nH_2O all exhibit featureless lineshapes representative of more disordered systems. The apparent centre-of-gravity shifts δ_{CG} suggest that each system is dominated by NbO_6 moieties; NbO_4 and NbO_5 species with ^{93}Nb linewidths typically ≥ 1 MHz are too broad to be detected by

Table 3. δ_{CG} and full width at half maximum of the NMR resonances for the different niobium oxides

Catalyst	δ_{CG} (ppm)	FWHM (ppm)
Nb_2O_5	-1260 ± 70	650 ± 70
HNb_3O_8	-1130 ± 40	400 ± 40
hy-Nb-TEOA	-1100 ± 60	600 ± 60
hy-Nb	-1100 ± 60	590 ± 60
meso Nb_2O_5	-1150 ± 90	920 ± 90

δ_{CG} and FWHM values were determined from corresponding Gaussian fittings of the NMR spectra.

single solid echo experiments. The width of the line shape for mesoporous Nb_2O_5*nH_2O is greater than for the other spectra, suggesting a greater structural disorder. Therefore, the ^{93}Nb NMR results follow the trend in crystallinity of Nb_2O_5/HNb_3O_8 > hy-Nb/ hy-Nb-TEOA > mesoporous Nb_2O_5*nH_2O, hence matching with the XRD and Raman results.

Due to the disordered nature of some of the NMR spectra it is difficult to derive the accurate NMR parameters. However, the centre of gravity of the chemical shift (δ_{CG}) of each line shape can be measured and is shown in Table 3. As seen, Nb_2O_5 has a significantly more negative δ_{CG} than the other niobium oxides. Similarly to the EXAFS result, this change in δ_{CG} could represent a trend in average oxidation state/coordination number from Nb^{5+} in Nb_2O_5 to an increase in Nb^{4+} character in the disordered materials.

Correlation of Structure and Acidity

In order to look at the relation between niobium oxide structure and acidity, a summary of the acidity measurements from our previously published work[56] is given in Table 4. Acid type (Brønsted versus Lewis), strength and quantity for each material have been probed by TMP ^{31}P NMR. TMP is an electron donor molecule that can form a stable adduct with an exposed cation (Lewis acid, LA) or proton (Brønsted acid, BA) of an oxide surface, via coordination of the P atom to the LA or BA center. Due to variations in the ^{31}P chemical shift (δ31P) of the surface TMP-LA and TMP-BA complexes, a differentiation between acid type and further strength is possible. For details on TMP ^{31}P NMR measurements, see Supporting Information.

Table 4. Surface area and acid site analysis for the different niobium oxides

Catalyst	Surface area ($m^2\,g^{-1}$)	Acid type and amount ($\mu mol\,g^{-1}$)	Acid site strength (ppm)
Nb_2O_5	3	ND	ND
HNb_3O_8	10	BA (30) no LA	BA: - 2.77
hy-Nb-TEOA	121	BA (171) LA (108)	BA: - 0.36 LA: - 24.98
hy-Nb	166	BA(259) LA(269)	BA: - 0.87 LA: - 42.27
meso Nb_2O_5	142	BA(338) LA(222)	BA: - 5.47 LA: - 25.37

Surface areas were obtained from BET measurements, Acid site analysis (qualitative and quantitative) by TMP ^{31}P NMR, BA region: ~0 to -6 ppm, LA region: ~-20 to -45 ppm, less negative ppm shift means stronger acidity within each region[57,58]

In general for solid acid metal oxides, BA sites are protonic surface sites in the form of strongly acidic bridging or terminal hydroxyl groups.[57,59] LA sites arise from the exposure of electron deficient metal centres, for example due to lower numbers or distortion of coordinating oxygens.[24,60] For Nb_2O_5 no acid sites are detected which is consistent from a structural point of view: protons giving rise to BA sites are not part of the crystal structure of H-Nb_2O_5. Further the rigid network of edge- and corner-sharing octahedra with a highly coordinated niobium centre makes the formation of LA sites/ TMP-LA adducts difficult. In addition, the general surface area of these bulk materials is low. The number of possibly formed LA sites from strongly distorted surface octahedra is thus not surprisingly below the detection limit. The same argument applies for HNb_3O_8 regarding LA site formation. BA sites/ TMP-BA adducts on the other hand are detected in this case, as expected due to the bulk layer structure consisting of alternating proton and niobate sheets.

If few-to monolayer hy-Nb and hy-Nb-TEOA were based on the exact same structural units as HNb_3O_8, an increase in BA sites according to surface area would be expected. However, in both cases the increase in BA sites is less pronounced (only about half) than expected from the increase in surface area (Table 4). Instead a large amount of LA sites is detected. It has been suggested that the removal of BA sites in form of water ($2H^+$ and $1O^{2-}$ from the Nb-O network) can result in the formation of LA sites.[5,60] Considering the fact that the reaction between two BA sites in form of a proton and a terminal hydroxyl group yields a water molecule and an oxygen vacancy, one accessible LA site (for TMP adsorption) is created (Scheme 3). This can explain the comparably low amounts of BA sites on hy-Nb and hy-Nb-TEOA, where during synthesis in the presence of stabilisers LA sites are created from the removal of BA

Scheme 3. Proposed oxygen vacancy/LA site formation *via* BA site removal in form of water

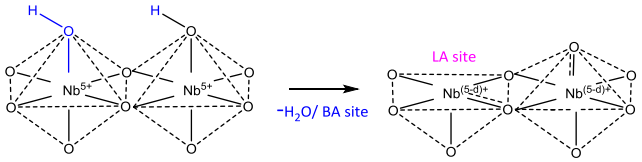

sites. The observed coordination numbers of below 6 (EXAFS) further support this type of LA site formation.

The above mechanism of water removal/LA site creation can already account for half the quantity of LA sites formed as BA sites removed. But significantly larger LA site quantities than expected from here were measured, indicating that the LA sites present do not entirely arise from the removal of BA sites. Other factors such as the removal of oxygen from Nb-O systems under reducing synthetic conditions (surfactants) likely play a role in LA site formation. As discussed earlier, the formation of oxygen vacancies during stabiliser synthesis could proceed via breakage of Nb---O bonds in the parent O=Nb---O

structure, which creates Nb^{4+} and allows free access for TMP-LA adduct formation (Scheme 4).

Scheme 4. Proposed oxygen vacancy/LA site formation *via* oxygen removal with Nb^{4+} formation and proton shift

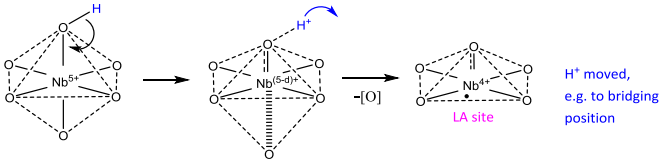

It is of further interest to note that the LA site strength of hy-Nb is lower than that of hy-Nb-TEOA (Table 4). This is likely due to the more pronounced Nb^{4+} character (XPS) of hy-Nb-TEOA with an overall lower coordination number (EXAFS), indicating more structural flexibility with more and stronger LA sites, possibly involving charge delocalization as discussed earlier. Previous analysis[8] on the mono-layer structure of hy-Nb-TEOA compared to few-layer hy-Nb also supports this increased structural flexibility and defect formation. At this point it should be noted that the lower acid site quantities and lower surface area measured for hy-Nb-TEOA compared to hy-Nb do not seem to agree with the above observations. However, a significant degree of re-stacking due to monolayer instability of hy-Nb-TEOA upon drying is likely to cause this deviation towards lower surface area and lower exposed than actual acid site quantities. It is to note that after the synthesis, the stabilizers (TEOA and ammonia) are removed by acid treatment.[56] For catalytic applications as discussed later, layer separation after acid treatment can re-stabilised in solution. In terms of BA site strength, hy-Nb-TEOA is more acidic than hy-Nb, which in turn is significantly more acidic than HNb_3O_8. This increase in acid strength for hy-Nb and further hy-Nb-TEOA could be caused by shifts in proton position along the Nb-O network upon few-to monolayer synthesis, where for example oxygen removal/LA site formation can induce such shifts to stronger bridging hydroxyl positions (Scheme 4).

Overall, it appears that the complexity of structural changes in hy-Nb and hy-Nb-TEOA compared to bulk HNb_3O_8 is the result of their high structural flexibility. At least two processes seem to be involved in LA site formation, where one mechanism gives rise to oxygen vacancies via the removal of two adjacent BA sites in form of water. Another mechanism of oxygen vacancy formation appears to proceed via the reduction process of O=Nb---O, which could further induce proton shifts as cause for the observed increased protonic strength (Scheme 5).

Scheme 5. Proposed oxygen vacancy/LA site formation upon downscaling from bulk HNb_3O_8 to few- to monolayer hy-Nb and hy-Nb-TEOA

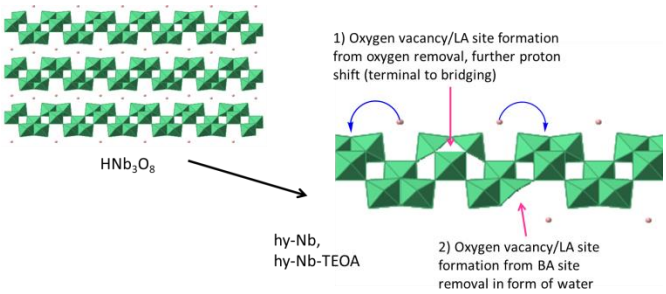

Mesoporous Nb_2O_5*nH_2O also shows large amounts of both BA and LA sites, which can be explained by its high surface area and structural flexibility as for the layered nano-materials. Its intrinsic porosity (TEM) with loose packing of most likely corner-sharing NbO_4, NbO_5 and NbO_6 units (EXAFS and XPS) is formed during etching/acid-soaking in the synthesis process. Resulting low coordination numbers and oxygen vacancies give rise to significant amounts of LA besides BA sites. The observed LA site strength is comparable to that of hy-Nb-TEOA, which goes in line with their similar properties regarding the increased Nb^{4+} character (XPS) and low coordination numbers (EXAFS). The comparatively low BA site strength suggests the presence of terminal rather than bridging hydroxyls[21,59], which supports a network consisting of lower connectivity corner-sharing more than edge-sharing Nb-O units (Scheme 6).

Scheme 6. Proposed LA and BA site origins in mesoporous Nb_2O_5*nH_2O

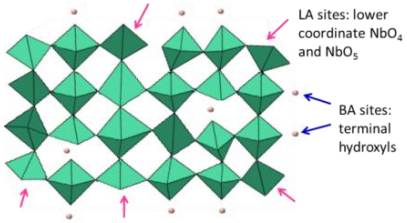

The different niobium oxides were tested with respect to their acid catalytic performance in glucose and fructose conversion to hydroxymethylfurfural (HMF) in water. The conversion of sugars to HMF over solid acids in water shows generally much lower yields than biphasic systems or ionic liquids, due to side reactions and product degradation.[61–63] However, due to the cost-, separation- and environment-friendly features of using just water as the solvent in combination with heterogeneous catalysts such as niobium oxides, these processes are worth-while of further investigation. As shown in our previous work, hy-Nb, hy-Nb-TEOA and mesoporous Nb_2O_5*nH_2O exhibit superior performance in glucose conversion with up to 36% HMF yield compared to bulk HNb_3O_8 and Nb_2O_5 (below 18% yield).[56] This can be related to the presence of LA sites on the nano materials, since LA sites catalyse glucose conversion to HMF much more efficiently than BA sites. It is suggested in literature that glucose conversion to HMF involves the LA catalysing isomerization to

fructose as important step before further conversion to HMF.[61,64–66] Fructose conversion to HMF on the other hand is a BA catalysed reaction, with the niobium oxides of weaker BA strength showing better performance, most likely due to reduced side reactions. Overall, mesoporous Nb_2O_5*nH_2O proved the best niobium oxide catalyst for glucose and fructose conversion (both 36% HMF yield), due to the presence of LA sites and its comparably weak BA sites.[56] Decent performance was also shown by hy-Nb (30% HMF yield), while the relatively weak BA catalyst HNb_3O_8 showed good results for fructose conversion (34% HMF yield) but performed worse for glucose (18% yield). We propose the following mechanisms for glucose to fructose isomerization over exposed Nb centres/LA sites and for fructose to HMF formation over BA sites/weaker terminal hydroxyls (Scheme 7).

Scheme 7. Proposed mechanisms for sugar conversion over niobium oxides

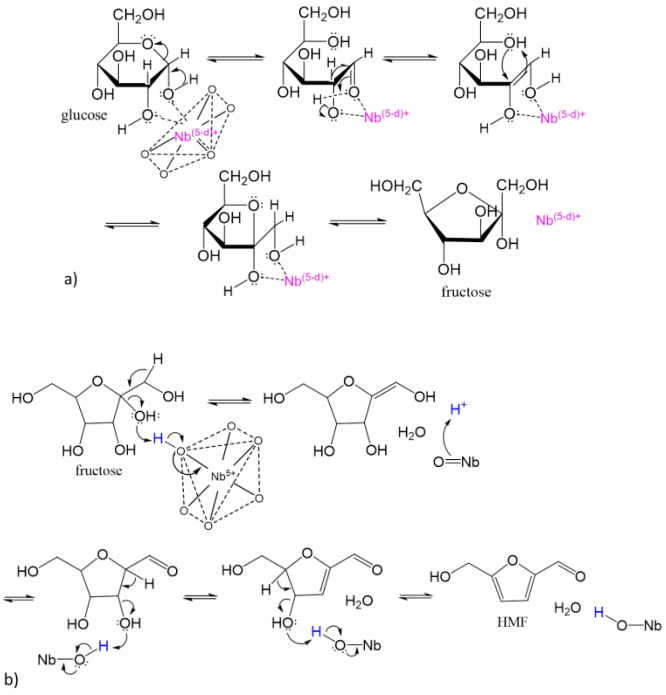

a) Glucose isomerization to fructose catalysed by exposed Nb centres/LA sites, b) Fructose conversion to HMF catalysed by weaker BA sites/terminal hydroxyls

Conclusions

Summing up all observations and conclusions made from the above structural analysis (XRD, TEM, Raman, XPS, EXAFS and NMR) supported by acid site analysis, the following characteristics stand out: the crystalline but low surface area/bulk materials Nb_2O_5 (H-Nb_2O_5) and HNb_3O_8 consist primarily of ordered edge- and corner-sharing NbO_6 octahedra with an average oxidation state of Nb^{5+}. Nb_2O_5 has a block structure with acid site quantities below the detection limit (TMP NMR), while HNb_3O_8 is made of layers of niobates interconnected by protons with detectable Brønsted acid (BA) sites as expected. Both Nb_2O_5 and HNb_3O_8 have been studied to detail in literature[1,5,8,33] and are therefore used for comparative study of the remaining niobium oxides. Hy-Nb and hy-Nb-TEOA have structural similarities to HNb_3O_8 but are few- to monolayered instead of bulk materials. It gives them higher surface areas and more structural flexibility with longer Nb-O bond distances and O=Nb---O species arising from distorted NbO_6. Large amounts of Lewis acid (LA) besides BA sites are detected and average coordination numbers of below 6 and a shift in oxidation state towards Nb^{4+} are observed. This points towards the presence of oxygen vacancies in hy-Nb and hy-Nb-TEOA, explaining the origin of the observed LA sites. These oxygen vacancies/LA sites are formed during synthesis in the presence of stabilizers, where one possible route involves the removal of BA sites in form of water with the simultaneous formation of NbO_5. Another route involves the removal of oxygen from elongated bonds as in O=Nb---O to form NbO_5, with the simultaneous formation of Nb^{4+} character and proton shifts, further reflecting the increased BA strength of hy-Nb and hy-Nb-TEOA. Overall, the flexible thin layer structures of hy-Nb and hy-Nb-TEOA consisting of NbO_6 units with distortions and defects, synthesized in the presence of stabilizers, give rise to large amounts of LA and BA sites compared to bulk layer HNb_3O_8. For mesoporous Nb_2O_5*nH_2O the structural analysis proves more difficult due to its highly amorphous nature, but some structural insights can still be obtained. The rather long and uniform Nb-O bond distances point towards a loosely packed structure consisting of mostly corner-sharing units. With an oxidation state shifted towards Nb^{4+} and an average coordination number of about 5, a mixed structure containing different species such as NbO_4, NbO_5 and NbO_6 is likely for mesoporous Nb_2O_5*nH_2O. Again large amounts of LA and BA sites are detected, due to the high porosity and loose network structure formed during acid-soaking in the synthesis process. LA sites show comparable acid strength to that of hy-Nb-TEOA and most likely arise from the lower coordinate NbO_4 and NbO_5 units. BA sites of comparably low strength support the presence of a lower connectivity corner- over edge-sharing network with terminal rather than bridging hydroxyls. With an overall better understanding of how acidity is related to structure, targeted synthesis becomes possible and solid acid catalysts meeting specific catalytic requirements can be developed.

ASSOCIATED CONTENT

Supporting Information. S1. Synthetic procedures of niobium oxides, S2. Surface area measurements, S3. TMP ^{31}P NMR analysis, S4. EXAFS measurements with k and R fittings.

This material is available free of charge via the Internet at http://pubs.acs.org.

AUTHOR INFORMATION

Corresponding Author

*edman.tsang@chem.ox.ac.uk

Notes

The authors declare no competing financial interest.

ACKNOWLEDGMENT

The authors would like to thank the EPSRC, UK and SINOPEC, China for financially supporting this research.

REFERENCES

(1) Nico, C.; Monteiro, T.; Graca, M. P. F. *Prog. Mater. Sci.* **2016**, *80*, 1.

(2) Ramakrishna, S.; Le Viet, A.; Reddy, M. V.; Jose, R.; Chowdari, B. V. R. *J. Phys. Chem. C* **2010**, *114* (1), 664.

(3) Schäfer, H.; Schulte, F.; Gruehn, R. *Angew. Chemie - Int. Ed.* **1964**, *76* (12), 536.

(4) Bach, D. **2009**, 210.

(5) Nowak, I.; Ziolek, M. *Chem. Rev.* **1999**, *99* (12), 3603.

(6) Fang, X.; Hu, L.; Huo, K.; Gao, B.; Zhao, L.; Liao, M.; Chu, P. K.; Bando, Y.; Golberg, D. *Adv. Funct. Mater.* **2011**, *21* (20), 3907.

(7) Katoh, R.; Furube, A.; Yoshihara, T.; Hara, K.; Fujihashi, G.; Takano, S.; Murata, S.; Arakawa, H.; Tachiya, M. *J. Phys. Chem. B* **2004**, *108* (15), 4818.

(8) Nakagawa, K.; Jia, T.; Zheng, W.; Fairclough, S. M.; Katoh, M.; Sugiyama, S.; Edman Tsang, S. C. *Chem. Commun.* **2014**, *50* (89), 13702.

(9) Tanabe, K. *Catal. Today* **2003**, *78* (1–4 SPEC.), 65.

(10) Ushikubo, T. *Catal. Today* **2000**, *57* (3–4), 331.

(11) Jehng, J.-M.; Wachs, I. E. *Chem. Mater.* **1991**, *3* (1), 100.

(12) Zhao, Y.; Zhou, X.; Ye, L.; Tsang, S. C. E. *Nano Rev.* **2012**, *3*, 17631.

(13) Iijima, S. *Acta Crystallogr. Sect. A* **1973**, *29* (1), 18.

(14) Anderson, J. S.; Browne, J. M.; Hutchison, J. L. *J. Solid State Chem.* **1972**, *5* (3), 419.

(15) Mcqueen, T.; Xu, Q.; Andersen, E. N.; Zandbergen, H. W.; Cava, R. J. *J. Solid State Chem.* **2007**, *180*, 2864.

(16) Marucco, J. F. *J. Chem. Phys.* **1979**, *70* (2), 649.

(17) Gatehouse, B. M.; Wadsley, A. D. *Acta Crystallogr. Sect. A* **1964**, *17*, 1545.

(18) Mertin, W.; Andersson, S.; Gruehn, R. *J. Solid State Chem.* **1970**, *1* (I), 419.

(19) Kato, K.; Tamura, S. *Acta Crystallogr. Sect. B* **1975**, *31* (3), 673.

(20) McConnell, A. A.; Aderson, J. S.; Rao, C. N. R. *Spectrochim. Acta Part A Mol. Spectrosc.* **1976**, *32* (5), 1067.

(21) Takagaki, A.; Lu, D.; Kondo, J. N.; Hara, M.; Hayashi, S.; Domen, K. *Chem. Mater.* **2005**, *17* (10), 2487.

(22) Murayama, T.; Chen, J.; Hirata, J.; Matsumoto, K.; Ueda, W. *Catal. Sci. Technol.* **2014**, *4*, 4250.

(23) Okuhara, T. *Chem. Rev.* **2002**, *102* (10), 3641.

(24) Nakajima, K.; Baba, Y.; Noma, R.; Kitano, M.; Kondo, J.; Hayashi, S.; Hara, M. *J. Am. Chem. Soc.* **2011**, *133*, 4224.

(25) Yang, Z. J.; Li, Y. F.; Wu, Q. Bin; Ren, N.; Zhang, Y. H.; Liu, Z. P.; Tang, Y. *J. Catal.* **2011**, *280* (2), 247.

(26) Xiong, J.; Wen, L.; Jiang, F.; Liu, Y.; Liang, S.; Wu, L. *J. Mater. Chem. A* **2015**, *3* (41), 20627.

(27) Lippmaa, E.; Samoson, A.; Magi, M. *J. Am. Ceram. Soc.* **1986**, *108* (8), 1730.

(28) Kunwar, A. C.; Turner, G. L.; Oldfield, E. *J. Magn. Reson.* **1986**, *69* (1), 124.

(29) R. Bodart, Jean-Paul Amoureux, Yves, P. *Mol. Phys.* **2000**, *98* (May 2017), 1545.

(30) Hanna, J. V.; Pike, K. J.; Charpentier, T.; Kemp, T. F.; Smith, M. E.; Lucier, B. E. G.; Schurko, R. W.; Cahill, L. S. *Chem. - A Eur. J.* **2010**, *16* (10), 3222.

(31) Lunsford, J. H.; Sang, H.; Campbell, S. M.; Liang, C. H.; Anthony, R. G. *Catal. Letters* **1994**, *27* (3–4), 305.

(32) Kao, H. M.; Yu, C. Y.; Yeh, M. C. *Microporous Mesoporous Mater.* **2002**, *53* (1–3), 1.

(33) Wang, S.; Liu, C.; Liu, L.; Zhang, X.; Gong, J.; Tong, Z. *Synth. React. Inorganic, Met. Nano-Metal Chem.* **2012**, *42* (2), 251.

(34) Hardcastle, F. D.; Wachs, I. E. *Solid State Ionics* **1991**, *45* (3–4), 201.

(35) Pittman, R. M.; Bell, A. T. *J. Phys. Chem.* **1993**, *97*, 12178.

(36) Hu, Z. P.; Li, Y. P.; Ji, M. R.; Wu, J. X. *Solid State Commun.* **1989**, *71* (10), 849.

(37) Grundner, M.; Halbritter, J. *J. Appl. Phys.* **1980**, *51* (1), 397.

(38) Koito, Y.; Rees, G. J.; Hanna, John, V.; Li, M. J. M.; Peng, Y.-K.; Puchtler, T.; Taylor, R.; Wang, T.; Kobayashi, H.; Teixeira, I. F.; Khan, M. A.; Kreissl, H. T.; Tsang, S. C. E. *ChemCatChem* **2017**, *9*, 144.

(39) Atashbar, M. Z.; Sun, H. T.; Gong, B.; Wlodarski, W.; Lamb, R. *Thin Solid Films* **1998**, *326* (1–2), 238.

(40) www.xpsfitting.com. No Titl.

(41) www.xpssimplified.com. No Title.

(42) Mrowec, S. *Ceramurg. Int.* **1978**, *4* (2), 47.

(43) Kodama, R.; Terada, Y.; Nakai, I.; Komaba, S.; Kumagai, N. *J. Electrochem. Soc.* **2006**, *153* (3), A583.

(44) Bizeto, M. A.; Leroux, F.; Shiguihara, A. L.; Temperini, M. L. A.; Sala, O.; Constantino, V. R. L. *J. Phys. Chem. Solids* **2010**, *71* (4), 560.

(45) Morante, J. R. **2002**, *853*, 2002.

(46) Morea, R.; Gonzalo, J.; Siegel, J.; Solís, J.; Optica, I. De. **2013**, 9.

(47) Oakton, E.; Tillier, J.; Siddiqi, G.; Mickovic, Z.; Sereda, O.; Fedorov, A.; Copéret, C. *New J. Chem.* **2016**, *40*, 2655.

(48) de Groot, F.; Vankó, G.; Glatzel, P. *J. Phys. Condens. Matter* **2009**, *21* (10), 104207.

(49) Ichikuni, N.; Sato, F.; Shimazu, S.; Uematsu, T. *Top. Catal.* **2002**, *18* (1), 101.

(50) Gasperin, M. *Acta Crystallogr. Sect. B* **1982**, *36*, 2024.

(51) Ravel, B.; Kelly, S. D. *AIP Conf. Proc.* **2007**, *882*, 150.

(52) Khabibulin, D.; Romanenko, K.; Zuev, M.; Lapina, O. *Magn. Reson. Chem.* **2007**, *45* (11), 962.

(53) Papulovskiy, E.; Shubin, A. a; Terskikh, V. V; Pickard, C. J.; Lapina, O. B. *Phys. Chem. Chem. Phys.* **2013**, *15* (14), 5115.

(54) Ashbrook, S. **2008**, 1.

(55) Satterlee, J. D. *Concepts Magn. Reson.* **1990**, *2* (3), 119.

(56) Kreissl, H. T.; Nakagawa, K.; Peng, Y. K.; Koito, Y.; Zheng, J.; Tsang, S. C. E. *J. Catal.* **2016**, *338*, 329.

(57) Chu, Y.; Yu, Z.; Zheng, A.; Fang, H.; Zhang, H.; Huang, S. J.; Liu, S. Bin; Deng, F. *J. Phys. Chem. C* **2011**, *115* (15), 7660.

(58) Zheng, A.; Huang, S.-J.; Liu, S.-B.; Deng, F. *Phys. Chem. Chem. Phys.* **2011**, *13* (33), 14889.

(59) Takagaki, A.; Tagusagawa, C.; Hayashi, S.; Hara, M.; Domen, K. *Energy Environ. Sci.* **2010**, *3* (1), 82.

(60) Corma, A. *Chem. Rev.* **1995**, *95* (3), 559.

(61) Van Putten, R. J.; Van Der Waal, J. C.; De Jong, E.; Rasrendra, C. B.; Heeres, H. J.; De Vries, J. G. *Chem. Rev.* **2013**, *113* (3), 1499.

(62) Rosatella, A. A.; Simeonov, S. P.; Frade, R. F. M.; Afonso, C. A. M. *Green Chem.* **2011**, *13* (4), 754.

(63) Teong, S. P.; Yi, G.; Zhang, Y. *Green Chem.* **2014**, *16* (4), 2015.

(64) Choudhary, V.; Mushrif, S. H.; Ho, C.; Anderko, A.; Nikolakis, V.; Marinkovic, N. S.; Frenkel, A. I.; Sandler, S. I.; Vlachos, D. G. *J. Am. Chem. Soc.* **2013**, *135* (10), 3997.

(65) Pagán-Torres, Y. J.; Wang, T.; Gallo, J. M. R.; Shanks, B. H.; Dumesic, J. A. *ACS Catal.* **2012**, *2* (6), 930.

(66) Assary, R. S.; Redfern, P. C.; Hammond, J. R.; Greeley, J.; Curtis, L. A. *J. Phys. Chem. B* **2010**, No. 114, 9002.

Insert Table of Contents artwork here